Chemical routes to materials

The nano-composite of Co-doped g-C$_3$N$_4$ and ZnO sensors for the rapid detection of BTEX gases: stability studies and gas sensing mechanism

Leqi Hu[1,2], Fuchao Jia[2,*] , Shuo Wang[1,2], Xingyan Shao[1,2], Xiaomei Wang[2], Yuping Sun[2], GuangChao Yin[2], Tong Zhou[2], Ramachandran Rajan[2], Zhenyu Feng[3,*], and Bo Liu[2]

[1] School of Material Science and Engineering, Shandong University of Technology, Zibo 255000, Shandong, China
[2] Laboratory of Functional Molecules and Materials, School of Physics and Optoelectronic Engineering, Shandong University of Technology, Zibo 255000, Shandong, China
[3] Key Laboratory for Colloid and Interface Chemistry of Education Ministry, School of Chemistry and Chemical Engineering, Shandong University, Jinan, Shandong 250100, People's Republic of China

ABSTRACT

In the present study, the nano-composite of Co-doped g-C$_3$N$_4$ and ZnO (Co–C$_3$N$_4$/ZnO) sensor was successfully prepared by using solid-phase precursor synthesis method. The crystalline phases were analyzed by X-ray diffraction (XRD), the microstructure of Co–C$_3$N$_4$/ZnO sensor was characterized by scanning electron microscopy (SEM) and transmission electron microscopy (TEM), and the chemical bonding states were analyzed by X-ray photoelectron spectroscopy (XPS). The gas sensing performance of Co–C$_3$N$_4$/ZnO sensor was systematically studied and compared with other sensors at the operating temperature of 200–370 °C, and the highest response was observed at 370 °C. Interestingly, Co–C$_3$N$_4$/ZnO sensor exhibited better response to o-xylene, m-xylene and p-xylene compared with other BTEX gases tested in this study; especially about 11 times higher response was observed against p-xylene compared with pure ZnO sensor at 370 °C. In addition, this sensor showed good stability and repeatability even after 14 weeks with a response/recovery time of 2 s/2 s. The improved gas sensing performance of this sensor was attributed to the formation of more active sites and more number of active oxygen species on the surface of ZnO. Based on these results, it could be ideal to explore Co–C$_3$N$_4$/ZnO sensor for the rapid detection of BTEX gases, specifically for p-xylene, in the surrounding environment.

🖄 Springer

Introduction

BTEX (benzene, toluene, ethylbenzene and xylene) gases, emitted by interior decoration, textile and other industries, greatly threaten people's health due to their neurotoxic nature and cause neurasthenia, anemia, leukemia and even death [1–11]. Importantly, BTEX gases are very difficult to be detected due to their low chemical activity and similar structures [12]. Therefore, it is of paramount importance to develop highly stable and efficient sensors for the rapid detection of BTEX gases.

Semiconductor metal oxides such as tin oxide (SnO$_2$) [13–16], titanium oxide (TiO$_2$) [17–19], zinc oxide (ZnO) [20–23] and indium oxide (In$_2$O$_3$) [24–26] were often used as the gas sensing materials. Among them, ZnO with a wide direct band gap of approximately 3.37 eV has attracted much attention of researchers owing to its high stability, easy preparation, non-toxic and harmless characteristics [27–29]. However, the gas sensing performances of ZnO to BTEX were not satisfied. For instance, the response value was lower than 5, the working temperature was often higher than 370 °C, and the response/recovery time was as long as tens of seconds or even minutes [6, 30–32]. These shortcomings restricted its applications in BTEX sensing. To cope with these problems, a variety of methods were developed to improve the gas sensing performance of ZnO-based sensors. Among them, loading noble metals was one of the most commonly used methods, and many researchers have used this method for the preparation of ZnO-based sensors. For instance, Shen et al. [33] loaded Au on porous ZnO rose-like architectures and detected xylene, and the gas sensing performance of this sensor was about eight times higher than that of pure ZnO. Similarly, when Pt–ZnO sensor was used to detect 50 ppm toluene, the response was found to be higher compared to ZnO sensor [34]. In another study, about 3.7 times higher response was observed when Pd nanoparticle-decorated ZnO nanorod was employed to detect toluene [35]. Despite these advantages, the noble metals tended to aggregate at higher temperatures, which, in turn, led to decreasing the number of active sites and may further influence the gas sensing performance of ZnO. In addition, the noble metals were costly and often caused secondary pollution. To overcome these disadvantages associated with the noble metals, researchers across the world were starting to explore non-noble metal materials to complex with ZnO.

Graphitic carbon nitride (g-C$_3$N$_4$) has been widely used in the field of photocatalysis due to its strong photochemical stability, high specific surface area and good catalytic ability [36–38]. Because of its n-type semiconductor characteristics, g-C$_3$N$_4$ was currently employed in gas sensing to provide more active sites for semiconductor metal oxides such as ZnO. Using g-C$_3$N$_4$, many studies have recently shown significantly improved gas sensing performance of ZnO-based sensors against different types of gases and solvents. For example, Li et al. [39] prepared ZnO–C$_3$N$_4$ sensor to detect CH$_4$; the gas sensing performance of this sensor was found to be about 2.2 times higher than that of pure ZnO. When polymer-wrapped g-C$_3$N$_4$ bundle-like ZnO nanorod was used to detect 100 ppm acetone, the response value was improved from 7 to 16 [40]. Similarly, significantly higher response was observed when ZnO–C$_3$N$_4$ sensor was used to detect 2000 ppm CH$_4$ under UV light at room temperature [41]. In recent times, the doping of transition metals like cobalt (Co) has been shown to further improve the catalytic activity of g-C$_3$N$_4$. The pyridine nitrogen group presented in g-C$_3$N$_4$ could capture Co^{2+} ions [42, 43], leading to the formation of Co–N bond, which, in turn, provided more number of reactive oxygen species to react with surrounding gas molecules [44–46]; thereby, it enhanced the gas sensing performance of the sensors. However, to the best of our knowledge, Co-doped C$_3$N$_4$ sensor has not yet been used for the detection of BTEX gases.

Hence, in the present study, a maiden attempt was made to prepare nano-composite of ZnO and Co-doped C$_3$N$_4$ sensor for the detection of BTEX gases. The gas sensing performance of this sensor was studied in comparison with ZnO, g-C$_3$N$_4$ and ZnO–C$_3$N$_4$ sensors. Finally, plausible mechanism for the improved gas sensing was proposed.

Experimental

Materials

Zinc acetate dihydrate (Zn(CH$_3$COO)$_2$·2H$_2$O) was purchased from Fuchen Chemical Reagent Factory of Tianjin (Tianjin, China). Urea (CO(NH$_2$)$_2$) and ethanol were purchased from Sinopharm Chemical

Reagent Co. Ltd. (Shanghai, China). Dicyandiamide ($C_2H_4N_4$) and cobalt chloride ($CoCl_2 \cdot 6H_2O$) were purchased from Aladdin Reagent (Shanghai) Co. Ltd., China. All chemicals were used directly without further purification.

Synthesis of porous Co–C$_3$N$_4$/ZnO

Porous ZnO nanosheet precursor

At first, zinc acetate (0.2 mol/L, 15 mL) and urea (0.4 mol/L, 15 mL) solutions were mixed well in a 50-mL beaker and dispersed for 10 min by ultrasonication. The mixture was transferred to a stainless steel high-pressure reactor having a capacity of 50 mL and heated in an oven at 120 °C for 5 h. The generated white precipitate was then washed with deionized water and ethanol thrice and dried at 60 °C for 12 h in the vacuum drying oven. Finally, the precursor of ZnO was obtained.

Co–C$_3$N$_4$

One gram of dicyandiamide (DCDA) was added into 20 mL of deionized water, and a certain amount of $CoCl_2 \cdot 6H_2O$ was added and then stirred. The mixture was placed in a water bath at 80 °C to remove water and then dried in the vacuum oven at 60 °C for 12 h. The dried sample was calcined in the tube furnace at 500 °C for 4 h under N_2 atmosphere. The sample obtained was called as Co–C$_3$N$_4$.

Co–C$_3$N$_4$/ZnO

300 mg of ZnO precursor and 100 mg of Co–C$_3$N$_4$ were ground in a mortar and then annealed in a muffle furnace at 400 °C for 2 h. The sample obtained was named as Co–C$_3$N$_4$/ZnO.

Characterization

The phases of as-prepared products were analyzed by X-ray diffraction (XRD, Bruker D8 Advance A25). The morphology and structure were studied using scanning electron microscopy (SEM, Quanta 250) and field emission transmission electron microscopy (FE-TEM, FEI Tecnai G2F 20, USA). The chemical elements and their valence states were obtained by X-ray photoelectron spectroscopy (XPS, Thermo Fisher Scientific Thermo ESCALAB 250Xi, USA).

Preparation and testing of gas sensors

The sample was ground in a mortar using anhydrous ethanol and then brushed on the ceramic tube. There were two gold electrodes at both ends of the ceramic tube and were connected with 2 Pt wires on each electrode. The sensor was heated by the nickel chromium wire present in the middle of the ceramic tube, and six wires were welded on the black base (Fig. 1a). The samples were tested in WS-30A gas sensor testing system after 5 days of aging (Fig. 1b). The response was defined as S = Ra/Rg, where Ra is the resistance of the gas sensor in the air and Rg is the resistance of the gas sensor in the test gas.

Results and discussion

Material characterization

The crystal structure and phase of the samples were studied using XRD, and the results are shown in Fig. 2. Pure g-C$_3$N$_4$ showed two different diffraction peaks at 13.1° and 27.4° corresponding to (100) and (002) planes [47]. After the introduction of cobalt into g-C$_3$N$_4$, the XRD pattern showed the peak intensity of (002) significantly decreased; it suggested that cobalt ions were embedded into in-planes of g-C$_3$N$_4$ [42, 48]. The crystal structure of ZnO was matched well with the JCPDS file no. 36–1451, and there was no redundant peak in the diffraction pattern of ZnO, indicating good crystallinity. For ZnO–C$_3$N$_4$, there was no peak corresponding to (100) crystal plane of g-C$_3$N$_4$. However, a tiny peak belonging to (002) of g-C$_3$N$_4$ was observed. This was attributed to the peak
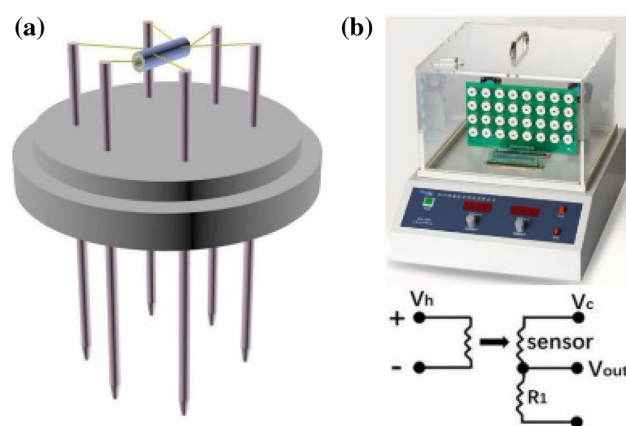
Figure 1 Scheme of gas sensor (**a**), gas sensing test system (**b**).
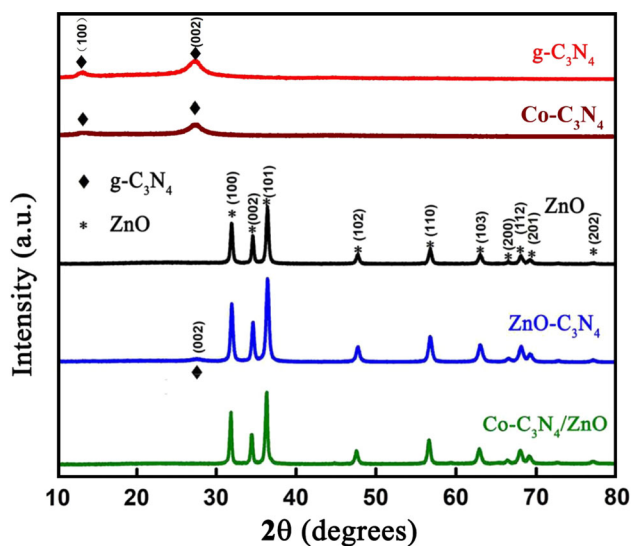
Figure 2 XRD patterns of ZnO, g-C$_3$N$_4$, Co–C$_3$N$_4$, ZnO–C$_3$N$_4$ and Co–C$_3$N$_4$/ZnO.

intensity of ZnO, which was too high to observe (100) peak of g-C$_3$N$_4$. In the case of Co–C$_3$N$_4$/ZnO, even the (002) peak of g-C$_3$N$_4$ was not seen (Fig. 2). It may be caused by the strong peak intensity of ZnO. Interestingly, in all the composites, the characteristic peak position of ZnO was not changed, indicating that there was no effect on ZnO structure even after the introduction of g-C$_3$N$_4$ or Co–C$_3$N$_4$.

As can be seen from Fig. 3a, b, ZnO had a porous sheet structure. The existence of pores increased the specific surface area of ZnO, which, in turn, increased its gas sensing performance. Figure 3b shows that the porous and flaky structure of ZnO was not changed after loading with g-C$_3$N$_4$; however, partial pores were observed. In good agreement with the SEM results, TEM images also showed the porous structure of ZnO nanosheets (Fig. 3c, d). Some of the holes were marked with red circles.

Figure 3e, f shows the HR-TEM images of Co–C$_3$N$_4$/ZnO, and the stripes are clearly marked in the images. In consistent with our XRD results, the lattice fringe spacing of 0.261 nm and the lattice spacing of 0.323 nm were corresponded to (002) plane of ZnO and (002) plane of g-C$_3$N$_4$ [49]. The elemental mapping results are shown in Fig. 3g–k. The distribution of each element was found to be relatively uniform, and no impurities were observed.

The chemical bonding states of different elements in Co–C$_3$N$_4$/ZnO were analyzed by using XPS, and the spectra are shown in Fig. 4. The Zn 2p spectrum

shown in Fig. 4b contained two typical peaks of Zn 2p, i.e., Zn 2p3/2 (1021.6 eV) and Zn 2p1/2 (1044.8 eV) with a splitting distance of 23.2 eV, indicating that Zn was present in the form of Zn^{2+} [50, 51]. As shown in Fig. 4c, O 1s was divided into two peaks located at 530.46 eV and 531.8 eV. These two peaks were attributed due to the presence of surface lattice oxygen and surface adsorbed oxygen [50, 52]. The latter's presence was crucial for the detection of BTEX gases. Similarly, the XPS spectrum of Co 2p also showed two peaks. One observed at 780.2 eV was due to the presence of Co–O bonding, and the other peak seen at 782.0 eV was caused by Co–N bonding (Fig. 4d). From these results, it can be speculated that Co has been doped into the interior of g-C$_3$N$_4$ [53, 54]. As shown in Fig. 4e, C 1s spectrum depicted three peaks at 288.9 eV, 284.7 eV and 286.5 eV corresponding to N–C=N, C–C and C=N groups [55, 56]. The different valence states of N are shown in Fig. 4f, which included C–N–H (401 eV), N–(C)$_3$ (399.79 eV), C=N–C (398.66 eV) and the pyridine N (398.18 eV) [52, 53].

Gas sensing performance of the synthesized sensors

The response value of different sensors against BTEX gases recorded at different temperatures is presented in Fig. 5a–c. In this study, the response value of sensors to BTEX $\bar{x}$ was found to be increased with the increase in temperature from 200 to 370 °C. Interestingly, Co–C$_3$N$_4$/ZnO sensor exhibited better response to BTEX compared with ZnO and ZnO–C$_3$N$_4$ sensors. The response values of Co–C$_3$N$_4$/ZnO sensor to benzene, ethylbenzene, toluene, o-xylene, m-xylene and p-xylene were 3($\pm$ 0.548), 8.5($\pm$ 0.99), 16.8($\pm$ 0.707), 21.3($\pm$ 0.67), 19.8($\pm$ 1.257) and 32.6($\pm$ 1.16), respectively. In addition, the results of standard deviation are summarized in Table S2. It can be clearly seen that the standard deviations of ZnO, ZnO–C$_3$N$_4$ and Co–C$_3$N$_4$/ZnO sensors were acceptable. Hence, three kinds of sensors had excellent repeatability to BTEX detection.

The responses of ZnO, ZnO–C$_3$N$_4$ and Co–C$_3$N$_4$/ZnO sensors to BTEX observed at 370 °C are shown in Fig. 5d. The response value of ZnO sensor to all the BTEX gases was found to be < 3. ZnO–C$_3$N$_4$ sensor also exhibited similar response value to benzene, toluene and ethylbenzene compared with ZnO sensor, while the response value of ZnO–C$_3$N$_4$ sensor for

Figure 3 SEM images of ZnO (**a**), ZnO–C₃N₄ (**b**); TEM images of Co–C₃N₄/ZnO (**c**, **d**); HRTEM images of Co–C₃N₄/ZnO (**e**, **f**); elemental mapping images of Zn, O, C, N, Co (**g**–**k**).
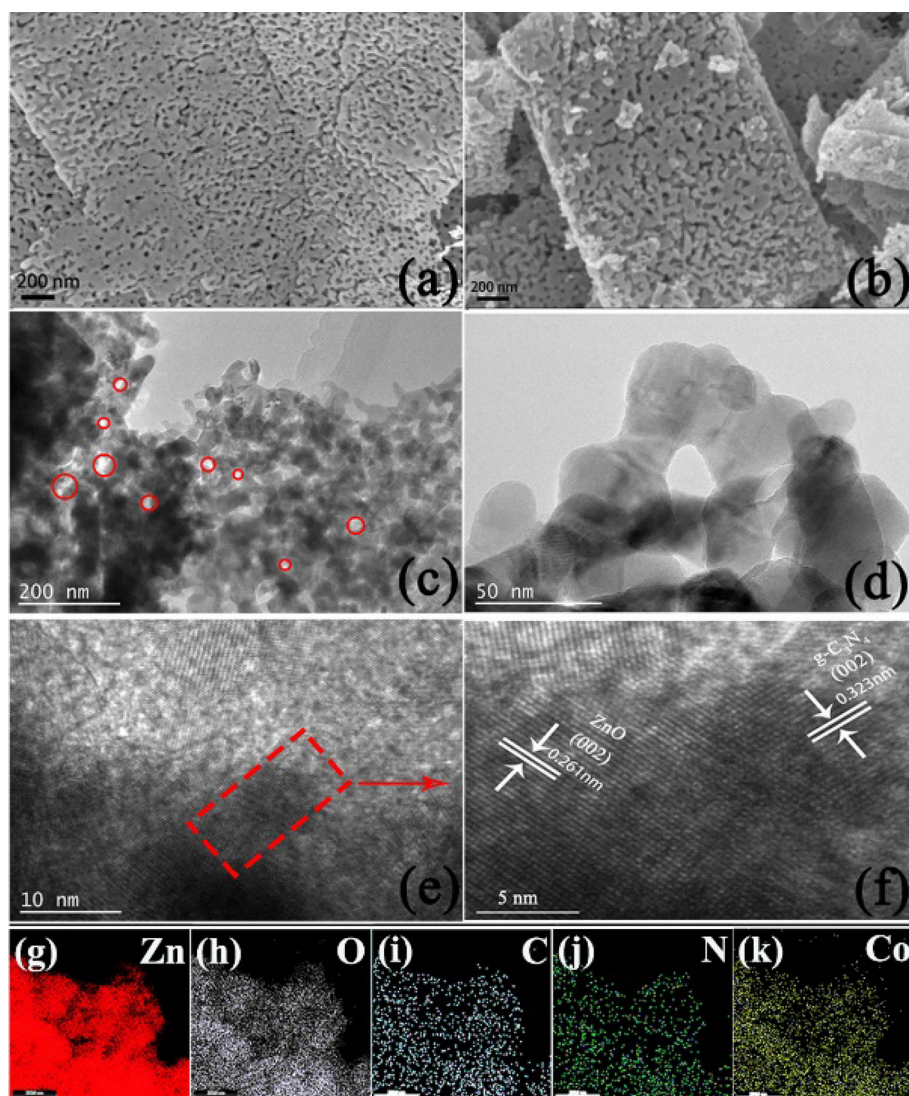
o-xylene, m-xylene and p-xylene was found to be about two times higher than that of pure ZnO sensor. In the case of Co–C₃N₄/ZnO sensor, the response value was significantly increased against all the gases except benzene; about 3–11 times higher response was observed compared with ZnO sensor. BTEX-sensing efficiency of Co–C₃N₄/ZnO sensor prepared in this study was compared with the previously reported sensors as listed in Table 1. Interestingly, our sensor outperforms most of other sensors in terms of response value. Among six different BTEX gases tested, Co–C₃N₄/ZnO sensor showed higher response to o-xylene, m-xylene and p-xylene, because the xylene molecules contained two methyl groups which may feature higher activation compared with benzene, toluene and ethylbenzene [57]. Therefore, o-xylene, m-xylene and p-xylene can be oxidized

easily that made it easier to the redox reaction [12]. Among three different xylene molecules tested, the highest response was recorded against p-xylene. In addition, the BTEX-sensing properties of three batches of Co–C₃N₄/ZnO were evaluated, and the results are shown in Fig. S4. The response value to each kind of BTEX for three batches of Co–C₃N₄/ZnO changed little at different temperatures. That indicated the different batches of Co–C₃N₄/ZnO had good repeatability to BTEX detection.

Figure 6a shows the response value of Co–C₃N₄/ZnO sensor at different concentrations of p-xylene ranging from 2 to 500 ppm at 370 °C. In this study, the response of the sensor changed so quickly when it was exposed to the target gas (p-xylene), which meant that the sensor had a quick response and recovering ability to p-xylene. Interestingly, a
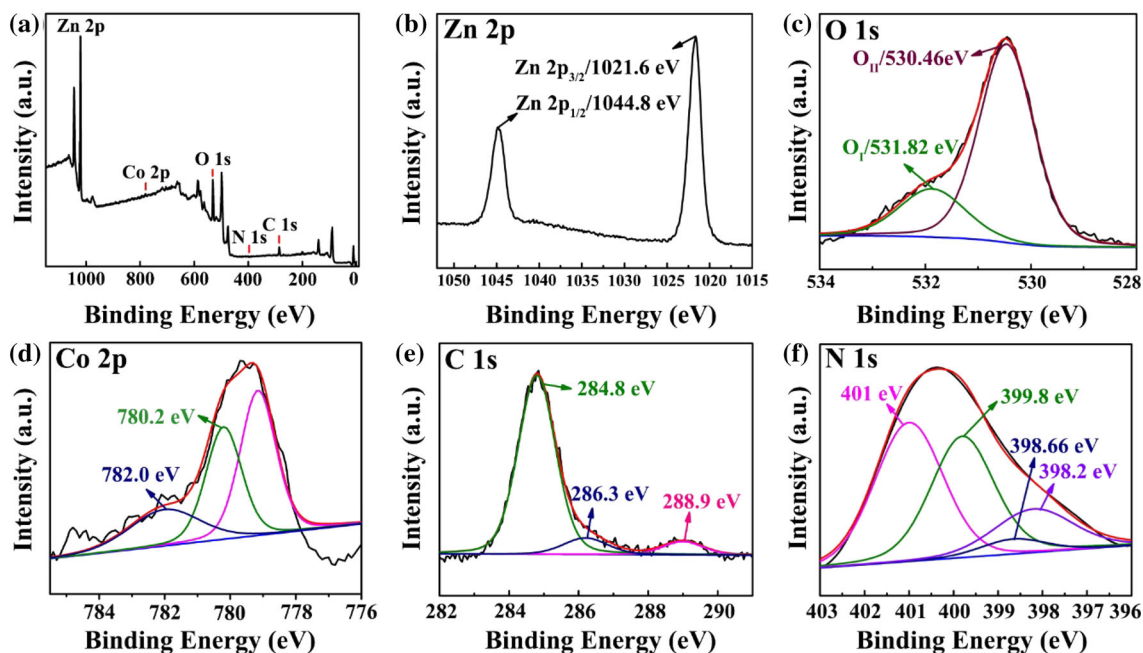
Figure 4 **a** XPS survey spectra of Zn 2p; high-resolution spectra of **b** Zn 2p, **c** O 1 s, **d** Co 2p, **e** C 1 s and **f** N 1 s in Co–C_3N_4/ZnO.

significant response was observed when the concentration of p-xylene was maintained at 2 ppm, indicating that Co–C_3N_4/ZnO sensor had excellent ability to detect even the lowest concentration of p-xylene tested in this study.

The linear curve for the response values of Co–C_3N_4/ZnO sensor is shown in Fig. 6b. It was obvious from this study that when the concentration of p-xylene was below 1000 ppm, the response of the sensor was found to be increased with the increasing concentrations of p-xylene. While the concentration of p-xylene was 1000 or 2000 ppm, the response value was basically unchanged, indicating that the adsorption ability of the sensor was saturated when the concentration of p-xylene reached 1000 ppm. When the sensor was exposed to lower concentrations (2–20 ppm) of p-xylene, the data obtained were very well fitted linearly with an R^2 value of 0.98788. (The corresponding linear fitting equation was y = 0.605x + 2.402. The standard error of intercept and slope was 0.545 and 0.047, respectively.)

Stability was another key factor that determines the real-world applications of the gas sensors. As shown in Fig. 6c, d, the response value of Co–C_3N_4/ZnO sensor to 100 ppm p-xylene was not changed much during the six successive cycles and after 10 days, indicating the excellent short-term stability and repeatability of Co–C_3N_4/ZnO sensor. The response/

recovery time of our sensor against p-xylene was only 2 s/2 s, much shorter than the studies reported to date [67, 68]. In addition, Co–C_3N_4/ZnO sensor also showed excellent long-term stability and repeatability even after 14 weeks (Fig. 6e).

Mechanism of gas sensing

When ZnO sensor was exposed to air, O_2 will be absorbed on the surface; the absorbed O_2 would capture electrons from the conduction band of ZnO, thus leading to the formation of active oxygen species such as O_2^- and O^-. The target gases would then react with the active oxygen species generated on the surface of ZnO. Finally, the active oxygen species would release the trapped electrons back to the conduction band of ZnO, and the specific reactions are given in Eqs. (1–3).

$$O_2 + e^- \rightarrow O_2^- \tag{1}$$

$$O_2^- + e^- \rightarrow 2O^- \tag{2}$$

$$C_aH_b + mO^{-n} \rightarrow aCO_2 + bH_2O + mne. \tag{3}$$
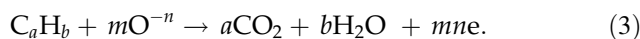
For composite material sensors, the electrons of g-C_3N_4 would migrate to the conduction band of ZnO owing to their difference in Fermi energy levels, which would lead to larger change of resistance and higher response. This can be attributed to the formation of more number of active oxygen species on
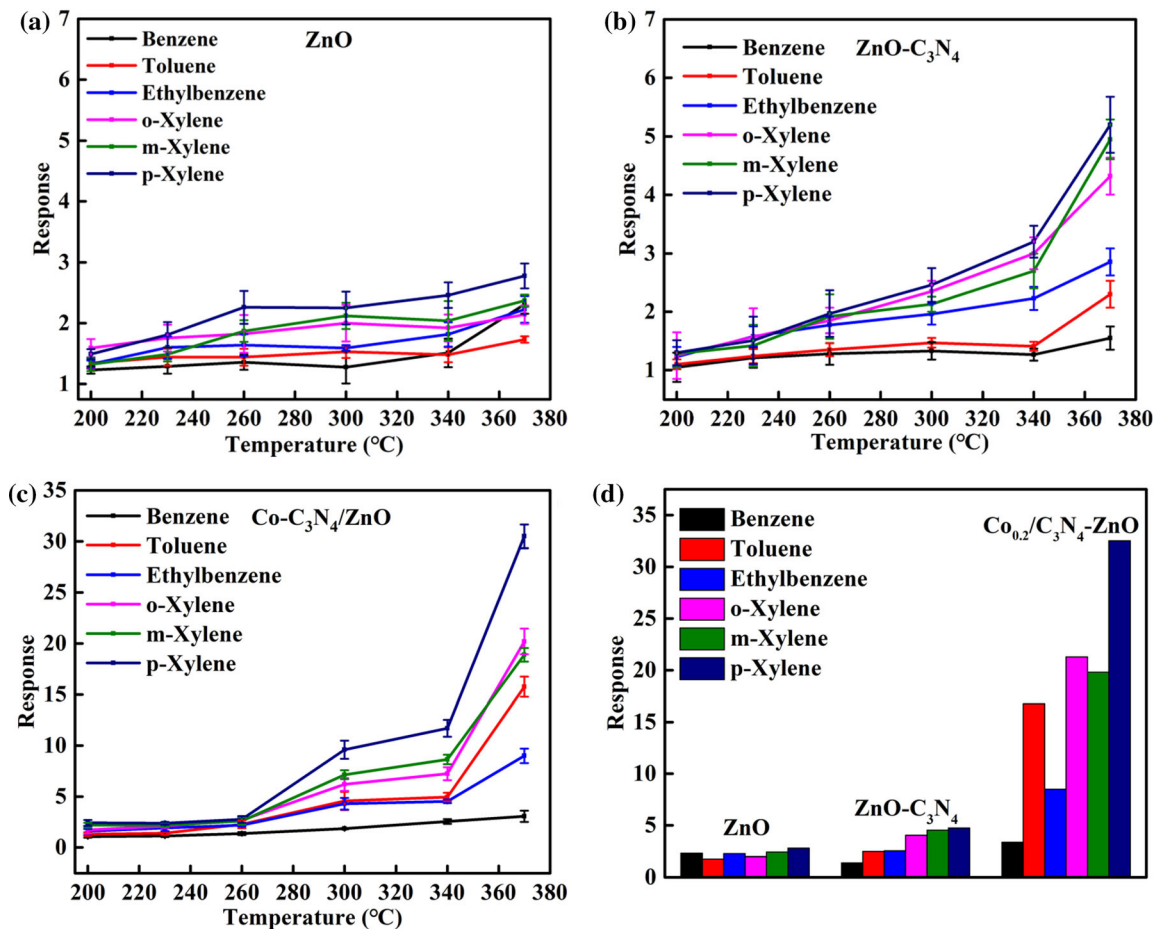
Figure 5 Response of the sensors: **a** pure ZnO, **b** ZnO–C$_3$N$_4$, **c** Co–C$_3$N$_4$/ZnO to 100 ppm BTEX at different operating temperatures, **d** responses of ZnO, ZnO–C$_3$N$_4$ and Co–C$_3$N$_4$/ZnO to 100 ppm BTEX at 370 °C (C$_3$N$_4$ and Co–C$_3$N$_4$ sensors did not show any response against BTEX). The error bar is the standard deviation, which was calculated from the equation: $S = \sqrt{\frac{\sum_{i=1}^{n}(x_i-\overline{x})^2}{n-1}}$, where x_i is the response value after each test, $\overline{x}$ is the average value and the number of repeats was 5.

Table 1 Comparison of BTEX-sensing performance of Co–C$_3$N$_4$/ZnO sensor with previously reported sensors

Materials	Conc. (ppm)	Temp. (°C)	Response	Ref
Composite of Co-doped C$_3$N$_4$ and ZnO	p-Xylene (100 ppm)	370	32.6	This work
Nanostructured ZnO thin films	Xylene (100 ppm)	Room temperature	2.25	[8]
Co-doped ZnO NFs	m-Xylene (100 ppm)	320	14.8	[58]
In-doped ZnO	Xylene (100 ppm)	420	10.5	[59]
Sb-doped ZnO	Xylene (100 ppm)	400	12	[60]
Zn–W–O nano-composite ceramics	Xylene (100 ppm)	425	7.3	[61]
Pd-decorated Bi$_2$O$_3$-ZnO	Toluene (200 ppm)	300	4	[62]
Mesoporous Fe$_2$O$_3$ nanostructures	Xylene (100 ppm)	340	6.5	[63]
WO$_3$ NMs	Xylene (1000 ppm)	300	2.6	[64]
CuO nanosheets	Xylene (100 ppm)	400	2.3	[65]
Au–NiO	Xylene (5 ppm)	400	3	[66]
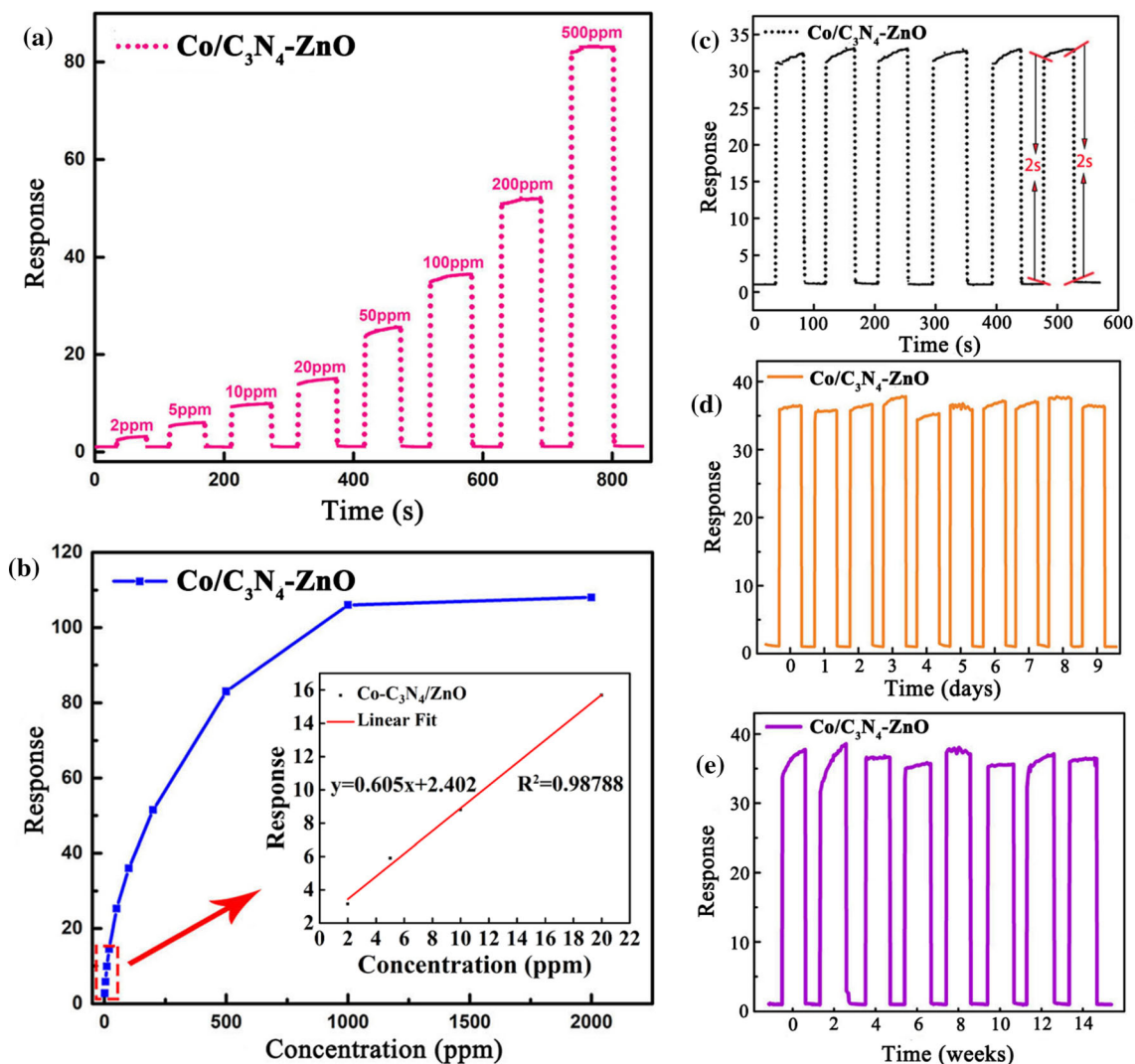
Figure 6 **a** Responses of Co–C$_3$N$_4$/ZnO sensor against different concentrations of p-xylene at 370 °C; **b** corresponding response curves of (a) (the inset shows the response curves of Co–C$_3$N$_4$/ZnO sensor against 2–20 ppm p-xylene); **c** six successive response cycles of Co–C$_3$N$_4$/ZnO sensor against 100 ppm p-xylene; the repeatability test of the sensor against 100 ppm p-xylene at 370 °C within **d** 10 days and **e** 14 weeks.

the surface of ZnO as discussed above (Fig. 7b). When ZnO was composited with Co–C$_3$N$_4$, Co and N would join and form Co–N bond, which then acted as a catalytic active center to promote the conversion of oxygen into active oxygen species [53]. As a result, more number of BTEX gases would react with active oxygen species; hence, more number of electrons would be released. Thereby, Co–C$_3$N$_4$/ZnO sensor, developed in this study, provides the best gas sensing performance against p-xylene than the so far reported sensors.

Conclusions

In the present study, the composite of porous ZnO nanosheet and Co-doped C$_3$N$_4$ was prepared by the precursor solid-phase synthesis method. And the gas sensing ability of this composite system was tested against BTEX gases. Interestingly, Co–C$_3$N$_4$/ZnO sensor exhibited better gas sensing performance to BTEX gases compared with pure ZnO sensor; notably, about 11 times higher response was observed against p-xylene along with much shorter rate of response/recovery time (2 s/2 s). In addition, this sensor had the ability to detect as low as 2 ppm of p-xylene and was found to be highly stable for up to

Figure 7 The gas sensing mechanism of **a** ZnO, **b** ZnO–C_3N_4 and **c** Co–C_3N_4/ZnO sensor.
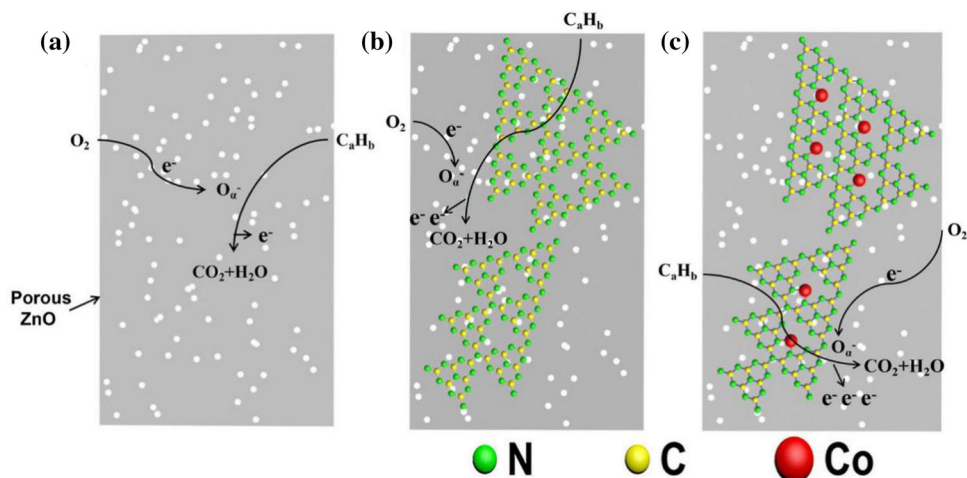
14 weeks. The higher efficiency of this sensor was likely due to the presence of more number of active sites and the formation of more number of active oxygen species on the surface of ZnO. Taken together, Co–C_3N_4/ZnO sensor could be ideal for the rapid detection of BTEX gases, especially for p-xylene, in the surrounding environment.

Acknowledgements

Compliance with ethical standards

Conflict of interest The authors declare that they have no competing financial interests or personal relationships that could have appeared to influence the work reported in this paper.

Electronic supplementary material: The online version of this article (https://doi.org/10.1007/s108 53-020-05614-2) contains supplementary material, which is available to authorized users.

References

[1] Zhang Y, Mu Y, Liu J, Mellouki A (2012) Levels, sources and health risks of carbonyls and BTEX in the ambient air of Beijing. China J Environ Sci 24(1):124–130

[2] Duarte-Davidson R, Courage C, Rushton L, Levy L (2001) Benzene in the environment: an assessment of the potential risks to the health of the population. Occup Environ Med 58(1):2–13

[3] Guo H, Lee S, Li W, Cao J (2003) Source characterization of BTEX in indoor microenvironments in Hong Kong. Atmos Environ 37(1):73–82

[4] Buczynska A, Krata A, Stranger M, Locateli Godoi A, Kontozova-Deutsch V, Bencs L (2009) Atmospheric BTEX concentrations in an area with intensive street traffic. Atmos Environ 43(2):311–318

[5] Dougherty D, Garte S, Barchowsky A, Zmuda J, Taioli E (2008) NQO1, MPO, CYP2E1, GSTT1 and GSTM1 polymorphisms and biological effects of benzene exposure–a literature review. Toxicol Lett 182(1–3):7–17

[6] Choudhury S, Feng Z, Gao C, Ma X, Zhan J, Jia F (2020) BN quantum dots decorated ZnO nanoplates sensor for enhanced detection of BTEX gases. J Alloys Compd 815:152376

[7] Liu Y, Wang L, Jin W, Zhang C, Zhou M, Chen W (2017) Synthesis and photocatalytic property of TiO_2@V_2O_5 core-shell hollow porous microspheres towards gaseous benzene. J Alloys Compd 690:604–611

[8] Nagaraju P, Vijayakumar Y, Ramana Reddy M (2019) Room-temperature BTEX sensing characterization of nanostructured ZnO thin films. J Asian Ceram Soc 7(2):141–146

[9] Chen Y, Wang L, Kong J, Shen B, Xu J (2020) Superhydrophobic hierarchical porous divinylbenzene polymer for

BTEX sensing and toluene/water selective detection. Chin Chem Lett 31(8):2125–2128

[10] Zhang D, Fan Y, Li G, Ma Z, Wang X, Cheng Z, Xu J (2019) Highly sensitive BTEX sensors based on hexagonal WO_3 nanosheets. Sens Actuators B 293:23–30

[11] Cho B, Lee K, Jo E, Kim J (2019) Detection of mixed BTEX with suppressed reaction specificity using Tin Oxide nanoparticles functionalized by multi-metalloporphyrins. IEEE Sens J 19(24):11791–11796

[12] Mirzaei A, Kim J-H, Kim HW, Kim SS (2018) Resistive-based gas sensors for detection of benzene, toluene and xylene (BTX) gases: a review. J Mater Chem C 6(16):4342–4370

[13] Zhang Z, YinYang CL, Jiang J, Guo Y (2019) Optimizing the gas sensing characteristics of Co-doped SnO_2 thin film based hydrogen sensor. J Alloys Compd 785:819–825

[14] Maheswari S, Karunakaran M, Chandrasekar LB, Kasirajan K, Rajkumar N (2020) Room temperature ammonia gas sensor using Nd-doped SnO_2 thin films and its characterization. J Mater Sci-Mater El 31(15):12586–12594. https://doi.org/10.1007/s10854-020-03809-6

[15] Chu X, Wang J, Zhang J, Dong Y, Sun W, Zhang W, Bai L (2017) Preparation and gas-sensing properties of SnO_2/-graphene quantum dots composites via solvothermal method. J Mater Sci 52(16):9441–9451. https://doi.org/10.1007/s10853-017-1148-9

[16] Ren F, Gao L, Yuan Y, Zhang Y, Alqrni A, Al-Dossary O, Xu J (2016) Enhanced BTEX gas-sensing performance of CuO/SnO_2 composite. Sens Actuators B 223:914–920

[17] Zhang M, Yuan Z, Song J, Zheng C (2010) Improvement and mechanism for the fast response of a Pt/TiO_2 gas sensor. Sens Actuators B 148(1):87–92

[18] Karthik P, Gowthaman P, Venkatachalam M, Rajamanickam A (2020) Propose of high performance resistive type H_2S and CO_2 gas sensing response of reduced graphene oxide/titanium oxide (rGO/TiO_2) hybrid sensors. J Mater Sci-Mater El 31(4):3695–3705. https://doi.org/10.1007/s10854-020-02928-4

[19] Yang W, Shen H, Min H, Ge J (2020) Enhanced acetone sensing performance in black TiO_2 by Ag modification. J Mater Sci 55(24):10399–10411. https://doi.org/10.1007/s10853-020-04703-6

[20] Yin M, Liu S (2014) Preparation of ZnO hollow spheres with different surface roughness and their enhanced gas sensing property. Sens Actuators B 197:58–65

[21] Sarf F, Er I, Yakar E, Acar S (2020) The role of rare-earth metal (Y, Ru and Cs)-doped ZnO thin films in NH_3 gas sensing performances at room temperature. J Mater Sci-Mater El 31(13):10084–10095. https://doi.org/10.1007/s10854-020-03554-w

[22] Jing Z, Zhan J (2008) Fabrication and gas-sensing properties of porous ZnO nanoplates. Adv Mater 20(23):4547–4551

[23] Wang D, Yin Y, Xu P, Wang F, Wang P, Xu J, Wang X, Li X (2020) The catalytic-induced sensing effect of triangular CeO_2 nanoflakes for enhanced BTEX vapor detection with conventional ZnO gas sensors. J Mater Chem A 8(22):11188–11194

[24] Zhang C, Huan Y, Sun D, Lu Y (2020) Synthesis and NO_2 sensing performances of CuO nanoparticles loaded In_2O_3 hollow spheres. J Alloys Compd 842:155857

[25] Wang H, Li H, Li S, Liu L, Wang L, Guo X (2016) Fabrication of hollow In_2O_3–ZnO microtubules by a simple biotemplate method and their gas-sensing properties. J Mater Sci-Mater El 28(1):958–962

[26] Yan S, Li Z, Li H, Wu Z, Wang J, Shen W, Fu Y (2018) Ultra-sensitive room-temperature H_2S sensor using Ag-In_2O_3 nanorod composites. J Mater Sci 53(24):16331–16344. https://doi.org/10.1007/s10853-018-2789-z

[27] Mei H, Zhou S, Lu M, Cheng L (2020) Tetrapod-like ZnO/$ZnFe_2O_4$ based heterostructure for enhanced ethanol detection. J Alloys Compd 840:155583

[28] Zhu L, Zeng W (2017) Room-temperature gas sensing of ZnO-based gas sensor: a review. Sens Actuators A 267:242–261

[29] Li C, Yu L, Yuan X, Li Y, Ning N, Cui L (2020) Ag nanorods assembled with ZnO nanowalls for near-linear high-response UV photodetectors. J Alloys Compd 830:154652

[30] Yu X, Song F, Zhai B, Zheng C, Wang Y (2013) Electrospun ZnO nanotubes and its gas sensing applications. Phys E 52:92–96

[31] Zhang L, Zhao J, Lu H, Gong L, Li L, Zheng J, Li H, Zhu Z (2011) High sensitive and selective formaldehyde sensors based on nanoparticle-assembled ZnO micro-octahedrons synthesized by homogeneous precipitation method. Sens Actuators B 160:364–370

[32] Du H, Li X, Yao P, Wang J, Sun Y, Dong L (2018) Zinc oxide coated tin oxide nanofibers for improved selective acetone sensing. Nanomater 8(7):509

[33] Shen Z, Zhang X, Ma X, Mi R, Chen Y, Ruan S (2018) The significant improvement for BTX (benzene, toluene and xylene) sensing performance based on Au-decorated hierarchical ZnO porous rose-like architectures. Sens Actuators B 262:86–94

[34] Gu C, Huang H, Huang J, Jin Z, Zheng H, Liu N (2016) Chlorobenzene sensor based on Pt-decorated porous single-crystalline ZnO nanosheets. Sens Actuators A 252:96–103

[35] Lou Z, Deng J, Wang L, Wang L, Fei T, Zhang T (2013) Toluene and ethanol sensing performances of pristine and

PdO-decorated flower-like ZnO structures. Sens Actuators B 176:323–329

[36] Singh J, Arora A, Basu S (2019) Synthesis of coral like WO$_3$/g-C$_3$N$_4$ nanocomposites for the removal of hazardous dyes under visible light. J Alloys Compd 808:151734

[37] Cao J, Qin C, Wang Y, Zhang H, Sun G, Zhang Z (2017) Solid-state method synthesis of SnO$_2$-decorated g-C$_3$N$_4$ nanocomposites with enhanced gas-sensing property to ethanol. Mater 10(6):604

[38] Yi F, Ma J, Lin C, Wang L, Zhang H, Qian Y (2020) Insights into the enhanced adsorption/photocatalysis mechanism of a Bi$_4$O$_5$Br 2/g-C$_3$N$_4$ nanosheet. J Alloys Compd 821:153557

[39] Li X, Li Y, Sun G, Luo N, Zhang B, Zhang Z (2019) Synthesis of a flower-like g-C$_3$N$_4$/ZnO hierarchical structure with improved CH$_4$ sensing properties. Nanomater 9(5):724

[40] Wang L, Liu H, Fu H, Wang Y, Yu K, Wang S (2018) Polymer g-C$_3$N$_4$ wrapping bundle-like ZnO nanorod heterostructures with enhanced gas sensing properties. J Mater Res 33(10):1401–1410. https://doi.org/10.1557/jmr.2018.37

[41] Xiao M, Li Y, Zhang B, Sun G, Zhang Z (2019) Synthesis of g-C$_3$N$_4$-decorated ZnO porous hollow microspheres for room-temperature detection of CH$_4$ under UV-light illumination. Nanomater 9(11):1507

[42] Wang X, Chen X, Thomas A, Fu X, Antonietti M (2009) Metal-containing carbon nitride compounds: a new functional organic-metal hybrid material. Adv Mater 21(16):1609–1612

[43] Deng S, Yuan P, Ji X, Shan D, Zhang X (2015) Carbon nitride nanosheet-supported porphyrin: a new biomimetic catalyst for highly efficient bioanalysis. ACS Appl Mater Inter 7(1):543–552

[44] Di Y, Wang X, Thomas A, Antonietti M (2010) Making metal-carbon nitride heterojunctions for improved photocatalytic hydrogen evolution with visible light. ChemCatChem 2(7):834–838

[45] Chen X, Zhang J, Fu X, Antonietti M, Wang X (2009) Fe-g-C$_3$N$_4$-catalyzed oxidation of benzene to phenol using hydrogen peroxide and visible light. J Am Chem Soc 131(33):11658–11659

[46] Jiang Y, Lu Y, Wang X, Bao Y, Chen W, Niu L (2014) A cobalt-nitrogen complex on N-doped three-dimensional graphene framework as a highly efficient electrocatalyst for oxygen reduction reaction. Nanoscale 6(24):15066–15072

[47] Liu W, Wang M, Xu C, Chen S (2012) Facile synthesis of g-C$_3$N$_4$/ZnO composite with enhanced visible light photooxidation and photoreduction properties. Chem Eng J 209:386–393

[48] Liu Q, Zhang J (2013) Graphene supported Co-g-C$_3$N$_4$ as a novel metal-macrocyclic electrocatalyst for the oxygen reduction reaction in fuel cells. Langmuir 29(11):3821–3828

[49] Adhikari S, Pant H, Kim H, Park C, Kim C (2015) Deposition of ZnO flowers on the surface of g-C$_3$N$_4$ sheets via hydrothermal process. Ceram Int 41(10):12923–12929

[50] Xing X, Xiao X, Wang L, Wang Y (2017) Highly sensitive formaldehyde gas sensor based on hierarchically porous Ag-loaded ZnO heterojunction nanocomposites. Sens Actuators B 247:797–806

[51] Postica V, Vahl A, Santos-Carballal D, Dankwort T, Kienle L, Hoppe M (2019) Tuning ZnO sensors reactivity toward volatile organic compounds via Ag doping and nanoparticle functionalization. ACS Appl Mater Inter 11(34):31452–31466

[52] Xie M, Tang J, Kong L, Lu W, Natarajan V, Zhu F (2019) Cobalt doped g-C$_3$N$_4$ activation of peroxymonosulfate for monochlorophenols degradation. Chem Eng J 360:1213–1222

[53] Deng L, Zhu M (2016) Metal–nitrogen (Co-g-C$_3$N$_4$) doping of surface-modified single-walled carbon nanohorns for use as an oxygen reduction electrocatalyst. RSC Adv 6(31):25670–25677

[54] Liang H, Wei W, Wu Z, Feng X, Mullen K (2013) Mesoporous metal-nitrogen-doped carbon electrocatalysts for highly efficient oxygen reduction reaction. J Am Chem Soc 135(43):16002–16005

[55] Hu J, Zou C, Su Y, Li M, Yang Z, Ge M (2017) One-step synthesis of 2D C$_3$N$_4$-tin oxide gas sensors for enhanced acetone vapor detection. Sens Actuators B 253:641–651

[56] Hu Y, Li L, Zhang L, Lv Y (2017) Dielectric barrier discharge plasma-assisted fabrication of g-C$_3$N$_4$–Mn$_3$O$_4$ composite for high-performance cataluminescence H$_2$S gas sensor. Sens Actuators B 239:1177–1184

[57] Xu T, Xu P, Zhneg D, Yu H, Li X (2016) Metal-organic frameworks for resonant-gravimetric detection of trace-Level xylene molecules. Anal Chem 88(24):12234–12240

[58] Liu L, Zhong Z, Wang Z, Wang L, Li S, Liu Z, Han Y, Tian Y, Wu P, Meng X (2011) Synthesis, characterization, and m-xylene sensing properties of Co–ZnO composite nanofibers. J Am Ceram Soc 94(10):3437–3441

[59.] Zhu B, Zeng D, Wu J, Song W, Xie C (2003) Synthesis and gas sensitivity of In-doped ZnO nanoparticles. J Mater Sci-Mater El 14:521–526

[60] Zhu B, Xie C, Zeng D, Song W, Wang A (2005) Investigation of gas sensitivity of Sb-doped ZnO nanoparticles. Mater Chem Phys 89(1):148–153

[61] Ge C, Xie C, Zeng D, Cai S (2007) Formaldehyde-, benzene-, and xylene-sensing characterizations of Zn–W–O

nanocomposite ceramics. J Am Ceram Soc 90(10):3263–3267

[62] Bonyani M, Lee J, Sun G-J, Lee S, Ko T, Lee C (2017) Benzene sensing properties and sensing mechanism of Pd-decorated Bi_2O_3-core/ZnO-shell nanorods. Thin Solid Films 636:257–266

[63] Li Y, Cao Y, Jia D, Wang Y, Xie J (2014) Solid-state chemical synthesis of mesoporous-Fe_2O_3 nanostructures with enhanced xylene-sensing properties. Sens Actuators B 198:360–365

[64] Chávez F, Pérez-Sánchez G, Goiz O, Zaca-Morán P, Pena-Sierra P, Morales-Acevedo A, Felipe C, Soledad-Priego M (2013) Sensing performance of palladium-functionalized WO_3 nanowires by a drop-casting method. Appl Surf Sci 275:28–35

[65] Yang C, Xiao F, Wang J, Su X (2015) 3D flower- and 2D sheet-like CuO nanostructures: microwave-assisted synthesis and application in gas sensors. Sens Actuators B 207:177–185

[66] Rai P, Yoon J-W, Jeong H-M, Hwang S-J, Kwak C-H, Lee J-H (2014) Design of highly sensitive and selective Au@NiO yolk-shell nanoreactors for gas sensor applications. Nanoscale 6(14):8292–8299

[67] Woo H-S, Kwak C-H, Chung J-H, Lee J-H (2014) Co-doped branched ZnO nanowires for ultraselective and sensitive detection of xylene. ACS Appl Mater Inter 6(24):22553–22560

[68] Sui L, Zhang X, Cheng X, Wang P, Xu Y, Gao S (2017) Au-loaded hierarchical MoO_3 hollow spheres with enhanced gas-sensing performance for the detection of BTX (benzene, toluene, and xylene) and the sensing mechanism. ACS Appl Mater Inter 9(2):1661–1670